Performance evaluation of electrochemical capacitors with activated carbon spheres as electrode material and aqueous electrolyte

Anetta Platek-Mielczarek, Joanna Conder, Krzysztof Fic, Camelia Matei Ghimbeu

Journal of Power Sources 542 (2022) 231714

Contents lists available at ScienceDirect

Journal of Power Sources

journal homepage: www.elsevier.com/locate/jpowsour

Performance evaluation of electrochemical capacitors with activated carbon spheres as electrode material and aqueous electrolyte

Anetta Platek-Mielczarek [a,b], Joanna Conder [c], Krzysztof Fic [a,*], Camelia Matei Ghimbeu [c,d,e,**]

[a] Poznan University of Technology, Institute of Chemistry and Technical Electrochemistry, Berdychowo 4, 60–965, Poznan, Poland
[b] Laboratory for Multiphase Thermofluidics and Surface Nanoengineering, Department of Mechanical and Process Engineering, ETH Zurich, Sonneggstrasse 3, Zurich, Switzerland
[c] Université de Haute-Alsace, Institut de Science des Matériaux de Mulhouse (IS2M), CNRS UMR 7361, F-68100, Mulhouse, France
[d] Université de Strasbourg, F-67081, Strasbourg, France
[e] Réseau sur le Stockage Electrochimique de L'Energie (RS2E), CNRS FR3459, 33 Rue Saint Leu, 80039, Amiens Cedex, France

HIGHLIGHTS

- The pyrolysis temperature affects the final morphology of the ACS sample.
- Surface chemistry and morphology impact the ACS electrode wettability.
- ACS can be used in asymmetric and symmetric cell construction.
- ACS show good charge propagation and capacitance retention an acidic and neutral medium.

GRAPHICAL ABSTRACT

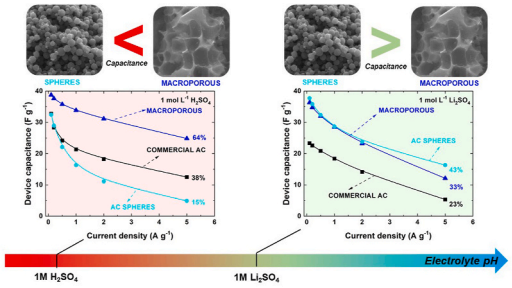

ABSTRACT

The model activated carbon spheres (ACSs) were optimized to be used as negative electrode in asymmetric electrochemical capacitors (ECs). A microporous commercial activated carbon was used as positive electrode.

Carbon spheres (CSs) were synthesized by precipitation polymerization at room temperature followed by pyrolysis and activation. By enhancing the carbon:KOH ratio from 1:2 to 1:4, an increase in the specific surface area from 380 $m^2\ g^{-1}$ to 2835 $m^2\ g^{-1}$ (1:4) was achieved along with an increase in pore volume/size. Consequently, the electrochemical performance in the aqueous electrolyte was improved. After activation, low-temperature-pyrolyzed polymer spheres (400 °C) result in random-like particles with macroporous structure, while intermediate- and high-temperature-pyrolyzed materials (550 °C and 700 °C) lead to partially and totally conserved spheres.

The interaction between the electrode material and electrolyte is important and is related to the texture, morphology, and surface chemistry of ACS. In 1 mol L^{-1} H_2SO_4, capacitance and rate handling are mostly affected by electrode morphology and wettability with the electrolyte. In 1 mol L^{-1} Li_2SO_4 electrolyte solution, texture and surface chemistry of the electrode material are crucial to obtain high-performance EC. Regardless of morphology, poor wetting properties of synthesized materials were found in Li_2SO_4, compared to the H_2SO_4 solution.

* Corresponding author.
** Corresponding author. Université de Haute-Alsace, Institut de Science des Matériaux de Mulhouse (IS2M), CNRS UMR 7361, F-68100, Mulhouse, France.
E-mail addresses: krzysztof.fic@put.poznan.pl (K. Fic), camelia.ghimbeu@uha.fr (C.M. Ghimbeu).

https://doi.org/10.1016/j.jpowsour.2022.231714
Received 9 November 2021; Received in revised form 30 May 2022; Accepted 31 May 2022
Available online 17 June 2022

1. Introduction

Currently, electrochemical capacitors (ECs) emerge as promising key energy storage devices for high power rates in our energy-driven lives [1]. However, due to the increasing environmental awareness, more attention is being devoted to sustainable EC components. Therefore, in the pursuit of inexpensive, ecological, sustainable and effective electrode materials, carbon materials attract immense interest in comparison to other classes of materials (metal oxides, metal nitrides, etc.). They demonstrate a well-developed surface area that guarantees high specific capacitance values. Their chemical, thermal, and electrochemical stability improves the durability of electrochemical devices in which they are implemented. One of the interesting carbon materials is spheroidal carbons, which can be classified as fullerenes, carbon onions (CO) [2,3], spheres (CS) [4] and beads (CB) [5]. Research concerning spherical carbons has gained increasing interest due to their unique morphology characterized by an inner and an outer (easily accessible) surface area. Spherical particles can possess a high degree of organization, i.e., graphitized particles (fullerenes, CO, CS) and more disordered highly microporous or macroporous particles (CS, CB). In addition, their controlled size might lead to more homogeneous electrode preparation and improved electrolyte diffusion. Therefore, such structures are widely studied in energy storage applications, especially batteries [6–9], ECs [10–13] or hybrid battery-capacitor devices [14]. To apply spheroidal carbon materials as anodes in Li-ion, Na-ion, or K-ion batteries [6–8], a high degree of graphitization is required [2,14], directly influencing their electrical conductivity. However, such an approach sacrifices the textural properties of carbon electrodes that are essential in EC application.

To enhance the texture of carbon (in particular microporosity), moderate pyrolysis temperatures (approximately 500–800 °C) are used [10–12,15]. Additionally, this process enables the preservation of heteroatom dopants in the structure [13,16–18]. For such purposes, nitrogen or sulfur are generally foreseen [9,19,20]. Open, hollow structures of CSs [10,21,22] or their composites with pseudocapacitive materials are advantageous [23–25] for EC application. Nevertheless, several crucial aspects of the CS synthesis process cannot be neglected. One approach involves hydrothermal carbonization with a temperature up to 250 °C instead of a direct pyrolysis step [26]. The most common precursors are carbohydrates (such as sucrose or glucose) or phenolic resins (phenol-formaldehyde) [26]. The latter, although their degree of carbonization is higher than the degree of carbonization of carbohydrates (40–50% *vs*. 20%), have questionable impacts on the environment. They release less gas during the carbonization process; however, their chemical nature is classified as highly toxic [18,27,28]. Undoubtedly, hazardous chemical substances (such as resorcinol or formaldehyde) allow the advancement of CS to be achieved, but improving the sustainability of EC remains a key challenge [16,17]. Unfortunately, considering each synthesis route, activation of the final product is required to obtain microporous carbons (ACSs) for EC application. Therefore, depending on the activation process, washing carbon with strong acidic [18,29–31] or alkaline solutions [27,28] is inevitable. Thus, it is important to minimize the environmental impact of the selected substrates, where possible [32].

CSs can use their external surface area simultaneously with the volume of the pores if they contain interconnected micro- and mesopores [12,29]. For this reason, the application of CS in ECs is readily studied – either as the main active electrode component or a support. Carbon spheres are investigated most often with alkaline electrolytic solutions, i.e., 6 mol L^{-1} KOH [9,10,22,33], however, acidic (1 mol L^{-1} H_2SO_4) [13,17,24] or neutral (1 mol L^{-1} Na_2SO_4) [12,21,34] are also used. The reported resistance values of CS electrodes are quite high, ranging from ca. 1 Ω [9,15,35–37] up to almost 8 ohms [12,21,25,30,31], depending on the electrolyte used. Despite having such equivalent series resistance values (ESR, recorded at 100 kHz) – CS presents satisfactory electrochemical performance in terms of its specific capacitance (ca. 200 F g^{-1} per electrode) and rate handling between 0.1 and 20 A g^{-1} (higher than 50%) [26]. Decreasing particle size was shown to increase specific capacitance [11,12,19,21,23,38]. Moreover, rate handling (specific capacitance ratio between high and low applied load, i.e., current, scan rate, power) seems to be affected by ACS particle size, their interconnection (presence of aggregates, free space between particles, etc.) and the bulk porosity of a singular particle [6]. Hence, rate handling recorded for ACS-based ECs varies from 50% [13,20,23] to 75% [10,22] in potentiodynamic studies. By tailoring the structure and texture of ACS, this metric still seems to be able to be improved. However, such investigations are quite often limited to three-electrode studies, in which CS-based EC device performance is not fully exploited.

Therefore, carbon spheres are still attractive and challenging materials because their various morphological, textural, and surface chemistry features can be designed and different synthesis protocols can be followed. Herein, we report on the full device performance of ACS-based ECs, and we demonstrate their great application potential in aqueous-based energy storage devices. Our research focuses on the synthesis of ACS using ecofriendly and non-carcinogenic precursors (phloroglucinol and glyoxylic acid). Optimization of the activation process and pyrolysis temperature allows the model ACS materials with tuned morphology, texture, surface functionalities to be obtained and their impact on the EC performance to be understood. For a fair comparison, two types of cell configurations were investigated: asymmetric (where ACS plays the role of a negative electrode active component) and symmetric configurations. Both were tested in acidic (1 mol L^{-1} H_2SO_4) and neutral (1 mol L^{-1} Li_2SO_4) aqueous electrolytic solutions. In acidic environments, because of the surface functionalities and structure of the material, macroporous materials exhibit a higher rate handling than spherical materials. In a neutral electrolytic solution, the ACS electrode performs better than macroporous or even commercial carbon cloth, showing how crucial proper electrode/electrolyte matching is in terms of their electrochemical performance. Successful improvement of ACS materials in terms of their electrochemical properties can be achieved by adjusting the pyrolysis temperature (here 550 °C) and/or optimizing the CS:KOH ratio in the activation process (here 1:3 by mass).

2. Experimental procedure

2.1. Materials synthesis

A scheme of activated carbon sphere synthesis is presented in Fig. 1. The process is based on the precipitation/polymerization of phenolic resin precursors in the presence of a cross-linker, followed by pyrolysis and activation of the polymer spheres obtained. The synthesis of the polymer spheres is described elsewhere [16,39] and involved dissolution under stirring of phloroglucinol (0.82 g) and glyoxylic acid (0.72 g) in 40 mL of ethanol. In addition, thiophene-2-carboxaldehyde (0.36 g) was used to provide a sulfur source. Next, a triethylenediamine (TEDA, 0.36 g) cross-linker was added to the solution to initiate the polymerization.

The as-obtained solution was kept without stirring for 48 h at 26 °C (*ageing* step).

Subsequently, after removal of excess solvent (either by centrifugation or decantation), the reddish-brown solid material was placed in crucibles and subjected to thermopolymerization in air at 80 °C overnight (16 h). Next, thermal treatment (pyrolysis) was performed at 400 °C, 550 °C or 700 °C with a temperature rate of 2 °C min^{-1} up to the maximum value and then held for 1 h in an Ar flow. During this step, the orange/red polymer resin spheres were converted to black carbon sphere material. The specific surface area of CS is expected to be below 500 m^2 g^{-1}; therefore, to increase the micropore content in CS, the activation process has been implemented [16]. CSs were mixed with KOH in a weight ratio of 1:2, 1:3, or 1:4; adding a few drops of distilled water allowed us to obtain a homogenous mixture in a mortar. When the CS:KOH ratio was studied, the samples were treated at fixed

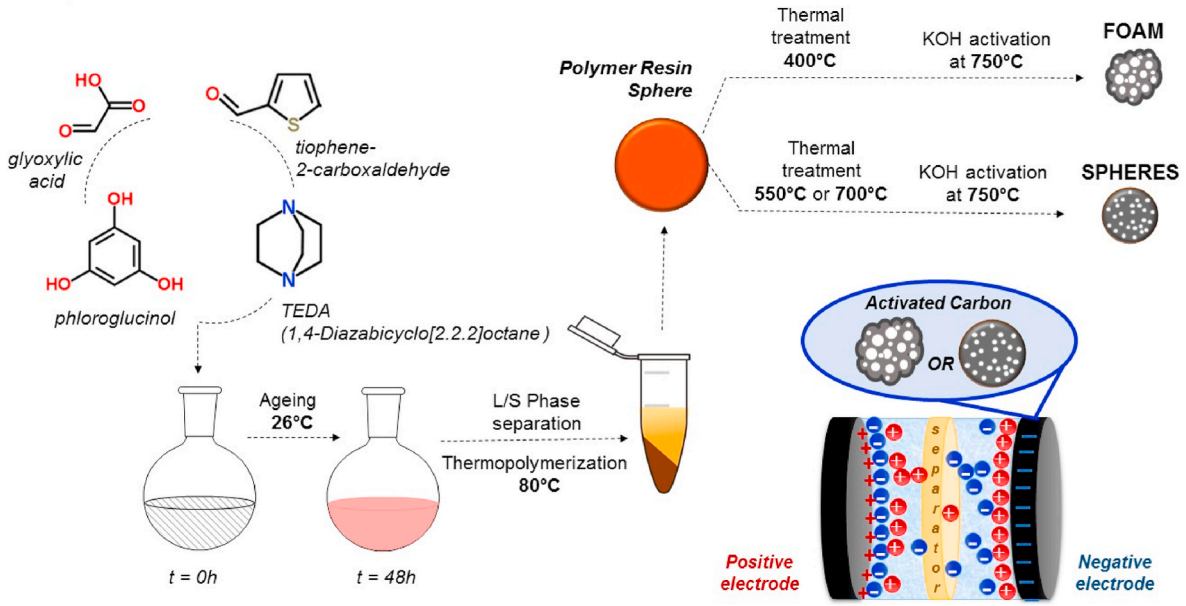

Fig. 1. Scheme of activated carbon sphere (ACS) synthesis.

temperatures, pyrolyzed at 700 °C, activated at 750 °C with a heating rate of 5 °C min^{-1} up to the maximum value and held for 1 h in an Ar flow. The activated samples obtained were labelled 1:2, 1:3 and 1:4 according to the CS: KOH ratio used. When the pyrolysis temperature (400 °C, 550 °C or 700 °C) was investigated, a constant CS:KOH ratio of 1:3 was fixed, and one activation temperature (750 °C) was used for all samples. The samples were labelled T-400, T-550 and T-700 according to the pyrolysis temperature applied.

During the activation step, an increase in the sample volume and a change in its morphology to fluffy powder were observed. The resulting material was then thoroughly washed with distilled water to remove KOH residues. In order to decrease the amount of acid used for washing, the second step includes washing with a mixture of HCl:H_2O at a 1:1 vol: vol ratio. The final washing step included hot water (80 °C) rinsing until the pH of the eluate became neutral. For the sake of comparison, one CS sample was pyrolyzed at 700 °C and was not activated (labelled N-A) to verify the textural and structural changes after the activation procedure.

2.2. Physicochemical characterization of materials

Synthesized carbon spheres were characterized in terms of their morphology, particle size distribution, texture, surface composition, wettability and conductivity. Morphology was examined using a FEI Quanta 400 scanning electron microscope (SEM) equipped with an energy dispersive analyzer (EDX), allowing determination of surface chemistry composition. The particle size distribution was evaluated using ImageJ software based on SEM micrographs. The textural properties of ACS were studied using N_2 adsorption at 77 K and CO_2 adsorption at 273 K using an ASAP 2020 apparatus (Micromeritics).

Prior to analysis, the samples were degassed under vacuum for 12 h at elevated temperatures (>100 °C). Next, gas adsorption isotherms were collected in the relative pressure range p/p_0 = 0–0.99 (N_2) and 0–0.03 (CO_2). The specific surface area was calculated using the Brunauer-Emmett-Teller (S_{BET}) equation in the relative pressure range 0.01–0.05. Cumulative surface area (S_{DFT}) from the 2D-NLDFT model was also noted for all samples. For pore size distribution, the 2D nonlocal density functional theory (2D-NLDFT) model for heterogeneous surfaces (with slit pores) was applied using SAIEUS software (Micromeritics) that allows micro- and mesopore volume calculation in the appropriate pore width range, based on a differential pore volume integral. Furthermore, V_{micro} was calculated using the Dubinin-Radushkevich equation, in the relative pressure range, P/P_0: 10^{-4}-10^{-2} for N_2 and CO_2, while V_{TOTAL} – at P/P_0: 0.99 and V_{meso} by $V_{TOTAL} - V_{micro}$. The average diameter of the micropore has been estimated based on a maximum peak in the micropore range (<2 nm) for both: N_2 and CO_2 adsorbates as discussed here [40] due to bimodal PSD in the micropore range. The supermicropore (from 0.8 to 2 nm) [41,42] volume was calculated by subtracting the micropore volume calculated from CO_2 adsorption from the value calculated from N_2 adsorption [43].

Surface chemistry was determined with X-ray photoelectron spectroscopy (XPS) on a VG ESCALAB 250 spectrometer using an Al K_α monochromatic source (15 kV, 15 mA) with a multidetection analyzer under a residual pressure of 10^{-8} Pa. The wetting properties of the prepared ACS electrodes were measured using contact angle techniques with a goniometer DSA100 (Krüss). The H_2SO_4 and Li_2SO_4 electrolytes were used. The conductivity of the ACS electrode materials (in the dry state) was evaluated using electrochemical impedance spectroscopy under open circuit conditions with a frequency of 100 kHz and an amplitude of ±5 mV.

2.3. Electrochemical characterization

For electrochemical investigations, electrode composites containing 90 wt % ACS, 5 wt % polymer binder (PTFE, 60 wt % water dispersion) and 5 wt % carbon black (C65 Timcal®, Cabot) were mixed in ethanol to form a homogenous paste. The electrode slurry was then rolled into a thin uniform film with an average thickness of 250 μm and cut into round discs with a diameter of 10 mm and an average mass of 10 mg.

The three-electrode setup used for material characterization provides excess electrolytic solution (approx. 10–20 mL). For this purpose, an oversized Pt mesh plays the role of a counter electrode and Hg| Hg_2SO_4 in the saturated K_2SO_4 – reference electrode (+0.650 V *vs.* NHE). The electrodes were tested with a 5 mV s^{-1} potential scan rate with a cut-off step of 100 mV for values lower than the open circuit potential. Such a protocol is assumed to resemble the operating conditions of the negative electrode. Next, the electrode was polarized towards higher potential values with the same scan rate. After the initial screening of the material using cyclic voltammetry, galvanostatic charge/discharge with a periodic relaxation period (so-called galvanostatic intermittent titration technique - GITT) was applied with a current

density of ±50 mA g^{-1}. This procedure allows a safe operational potential range of the ACS electrode to be determined.

Microporous activated carbon (AC) used in asymmetric capacitors was a binder-free carbon cloth (KYNOL 507–20, Kynol GmbH) cut into round discs with a diameter of 10 mm and an average electrode mass similar to ACS electrodes. In the asymmetric and symmetric full-cell studies, electrodes were separated by a glass fibre membrane (Whatman GF/A® 260 μm thick) soaked with ca. 150 μL of electrolyte. Because of the stable performance of the ACS electrode material in cathodic conditions – proven by 3-electrode measurements - it has been applied primary as a negative electrode. Microporous activated carbon plays a positive role in the asymmetric configuration. Systems were tested with 1 mol L^{-1} H_2SO_4 or 1 mol L^{-1} Li_2SO_4 aqueous solutions in the voltage range 0–0.8 V. Implemented techniques include cyclic voltammetry with a scan rate of 1–100 mV s^{-1}, galvanostatic charge/discharge with a current density of 0.1–5 A g^{-1}, and electrochemical impedance spectroscopy at 0 V in the frequency range of 1 mHz–100 kHz with an amplitude of ±5 mV. Calculated rate handling is the percentage ratio between specific capacitance calculated at high (5 A g^{-1}) and low current density (0.1 A g^{-1}) from potentiodynamic studies or the ratio between specific capacitance calculated at low frequency (1 mHz) and high frequency (1 Hz) in impedance spectroscopy, providing information about the system capability to deliver energy in the shortest period; thus, it is a metric related to the power response.

All electrochemical parameters presented in the manuscript are expressed per cell, i.e., the total mass of both electrodes. Notably, specific capacitance calculations were performed by integrating discharge curves. Additionally, ACS exhibiting the best electrochemical performance was implemented in a symmetric cell and tested with both: 1 mol L^{-1} H_2SO_4 and 1 mol L^{-1} Li_2SO_4.

3. Results and discussion

3.1. Impact of activation on carbon properties and electrochemical performance

To optimize CS synthesis, we thoroughly investigated the activation step. Three weight ratios of CS to KOH (activation agent) were applied: 1:2, 1:3 and 1:4 and compared to the nonactivated sample (N-A).

SEM micrographs (Fig. 2A and Figs. S1 and SI) present the spherical shape of carbon particles pyrolyzed at 700 °C and KOH-activated at 750 °C with various CS:KOH ratios. To quantify the morphology of the samples, the particle size distributions were determined using ImageJ software for at least 10 micrographs with various magnifications [44]. Regardless of the CS:KOH ratio, the spherical shape of the particles is preserved. Hence, the activation agent itself and its quantity do not influence the morphology of the carbon samples, but lead to a slight widening of the particle size distribution. The average particle sizes found were 2.9 μm (N-A), 2.8 μm (1:2), 2.9 μm (1:3) and 2.6 μm (1:4) (Fig. 2B).

N_2 and CO_2 adsorption isotherms were recorded to characterize the porous texture of the materials (Fig. 3). The N_2 adsorption/desorption isotherms show a type I shape specific to microporous materials. An important increase in N_2 adsorbed volume is observed for ACS compared to nonactivated ACS (N-A). The increase in the CS:KOH ratio has an impact on the adsorbed volume of N_2, which is enhanced in the relative pressures.

The textural characterization of carbon spheres pyrolyzed at 700 °C (N-A) and subsequently activated using various CS:KOH ratios is presented in Table 1 together with the data for commercial AC, used as a positive electrode in the asymmetric device.

The AC material is highly microporous and contains mostly micropores. The N-A sample demonstrates a very low specific surface area and, thus, was not considered for further tests. Although the morphology of the samples is similar, their texture differs noticeably. When increasing the CS:KOH ratio, one can observe an increase in BET specific surface area from 1610 m^2 g^{-1} (1:2) to 2070 m^2 g^{-1} (1:3) and up to 2835 m^2 g^{-1} (1:4). Sample 1:2 shows textural properties comparable to the textural properties of microporous AC, whereas the other two samples, i.e., 1:3 and 1:4, surpass the AC values. Increasing the CS:KOH ratio, the mesopore fraction also increases from 0.01 cm^3 g^{-1} (1:2) to 0.05 cm^3 g^{-1} (1:3) and up to 0.14 cm^3 g^{-1} (1:4). Therefore, it is assumed that the sample exhibiting a significant volume of mesopores (1:4) is able to demonstrate a satisfactory rate capability and high-power response [45]. To verify and characterize the micropore texture in more detail, CO_2 adsorption was also carried out at 273 K, as it allows the calculation of the micropore volume [46]. Interesting observations concerning the CO_2 as an adsorbate and its role in discrimination of certain pore diameters are reported elsewhere [47]. Activation significantly increases the volume of micropores determined by CO_2 adsorption independent of the carbon:KOH ratio (0.15 cm^3 g^{-1} for N-A and 0.75 cm^3 g^{-1} for 1:2 sample). Compared to AC material, 1:3 and 1:4 ACS contains a considerable volume of supermicropores. It appears that AC contains a negligible amount of supermicropores, proving its narrow pore size distribution, similarly to N-A and 1:2 ACS. ACS 1:3 and 1:4 samples have higher supermicropore volumes than AC, 0.25 cm^3 g^{-1}, 1:4–0.33 cm^3 g^{-1}, respectively.

It appears that the activation process increases the volume of micropores determined by both N_2 and CO_2, together with the average diameter of the micropore (L_0). For the N-A sample, the maximal micropore diameter with the highest contribution from the micropores equals 0.57 nm, increasing to 0.63, 0.69 and 0.83 nm for the 1:2, 1:3, and 1:4, respectively (from N_2 adsorption).

While considering CO_2 as an adsorbate, one can observe an increase

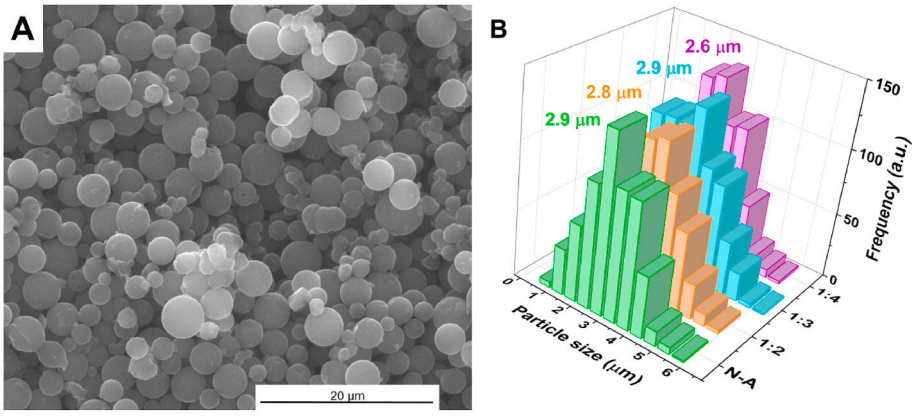

Fig. 2. CS pyrolyzed at 700 °C and subsequently activated at 750 °C using different CS:KOH mass ratios: A) SEM micrograph for 1:2 sample; B) particle size distribution for all CS:KOH ratios.

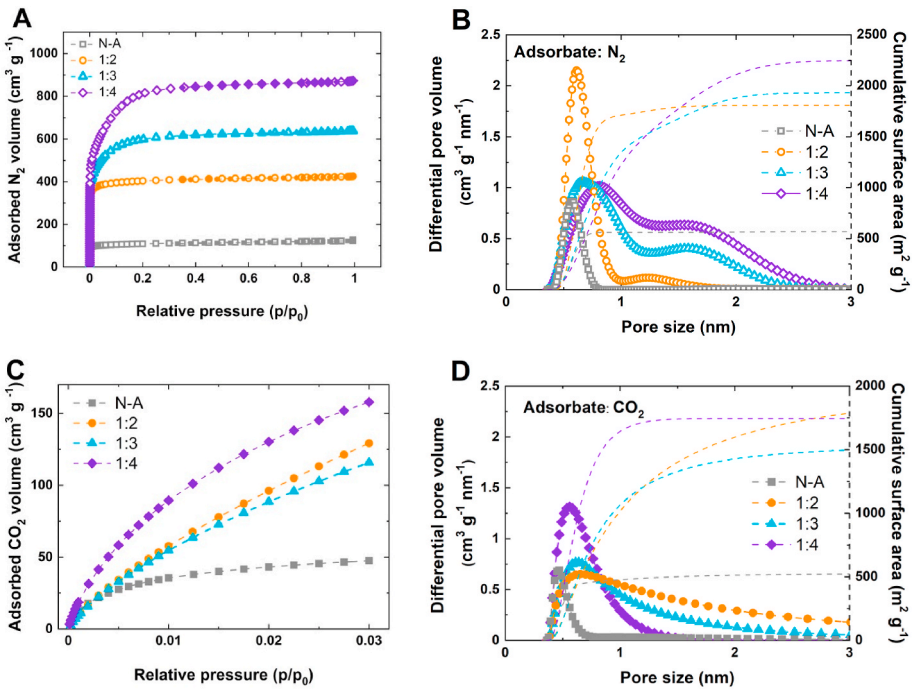

Fig. 3. N_2 adsorption data for nonactivated carbon spheres (N–A) and activated carbon spheres with different CS:KOH ratios: 1:2, 1:3 and 1:4: A) isotherms; B) pore size distribution with cumulative surface area evolution. Corresponding CO_2 adsorption data: C) isotherms; D) pore size distribution with cumulative surface area evolution.

Table 1
Textural properties of commercial AC and CS pyrolyzed at 700 °C (N-A) and subsequently activated at 750 °C using different CS:KOH mass ratios: 1:2, 1:3, and 1:4.

Sample	N_2 adsorption at 77 K						CO_2 adsorption at 273 K		$V_{SUPERMICRO}$ cm^3 g^{-1}
	S_{BET} m^2 g^{-1}	S_{DFT} m^2 g^{-1}	V_{TOTAL} cm^3 g^{-1}	V_{MICRO} cm^3 g^{-1}	V_{MESO} cm^3 g^{-1}	Micropore size at peak maximum, nm	V_{MICRO} cm^3 g^{-1}	Micropore size at peak maximum, nm	
AC	1840	1620	0.69	0.69	0.00	0.83	0.65	0.81	0.04
N-A	380	575	0.20	0.17	0.03	0.57	0.15	0.46	0.02
1:2	1610	1813	0.62	0.61	0.01	0.63	0.75	0.64	n/a
1:3	2070	1930	0.90	0.85	0.05	0.69	0.60	0.63	0.25
1:4	2835	2245	1.25	1.08	0.14	0.83	0.57	0.56	0.33

in L_0 for activated samples, following the trend slightly different from that determined by using N_2. For aqueous electrolytic solutions, it is assumed that a 0.7-nm pore diameter is optimal for the formation of electric double layers [48]. The average micropore size increases with the carbon:KOH ratio, and also its pore size distribution becomes wider (as observed in the broad tail in Fig. 3B and **D**).

ACS samples 1:2, 1:3 and 1:4 were tested as negative electrodes in aqueous ECs (with 1 mol L^{-1} Li_2SO_4) for comparison with the symmetric AC:AC system and to verify their electrochemical application potential, as presented in Fig. 4. The asymmetric configuration results from high cathodic stability of ACS material recorded in the three-electrode setup (explained in the Experimental section).

Fig. 4A presents galvanostatic charge/discharge curves recorded at 0.1 A g^{-1}. For all tested cells, the triangular shape of the voltage profile indicates that the main charge storage mechanism is based on the electrostatic attractions between the carbon electrode and the electrolyte-originating ions. Nevertheless, the calculated energetic charge/discharge efficiency clearly indicates that a certain part of the charge delivered to the system cannot be recovered. The highest energetic efficiency of 95% was found for the AC:AC system, which indicates almost perfect reversibility of the charging/discharging process owing to the optimal correlation between textural properties, morphology and surface chemistry (92.30 at % of C and 7.65 at % of O from Ref. [49]). ACS systems show energetic efficiencies of 86% (1:2), 82% (1:3) and 84% (1:4).

Fig. 4B presents specific capacitance values for various applied current densities. Despite the fact that sample 1:2 shows a moderate surface area (S_{BET} = 1610 m^2 g^{-1}), it does not guarantee well-developed EDL formation, as its mesoporosity is limited and the pore size distribution is too narrow (0.63 nm *vs* optimal 0.7 nm) [48–50] to provide a high specific capacitance in aqueous electrolytic solutions. The rate handling for this system (1:2) under the investigated current loads was 14%. Increasing the CS:KOH ratio to 1:3 and 1:4 already introduces additional micropore volume to obtain higher specific capacitance by +65% (38 F g^{-1} for 1:3) and +70% (39 F g^{-1} for 1:4) than for the AC system at 0.1 A g^{-1} (23 F g^{-1}). This improvement is in accordance with the evolution of the increase in specific surface area and the distribution of pore size with the micropore diameter L_0 (AC- 0.83 nm, ACS 1:3–0.67 nm and 1:4–0.80 nm) (Table 1). The limit for the S_{BET} value seems to be around 2000 m^2 g^{-1}; beyond this value, no great improvement in specific capacitance was found, especially with L_0 wider than 0.7 nm, considered the best pore size for energy storage in aqueous electrolytes [48,50,51]. It proves that the electrochemical accessible area is a key factor, not the developed specific surface area itself. Furthermore, the rate handling is promising, that is, for the 1:3 sample - 43%, which is a higher value than for the AC system (23%). Sample 1:4 demonstrates the highest mesopore

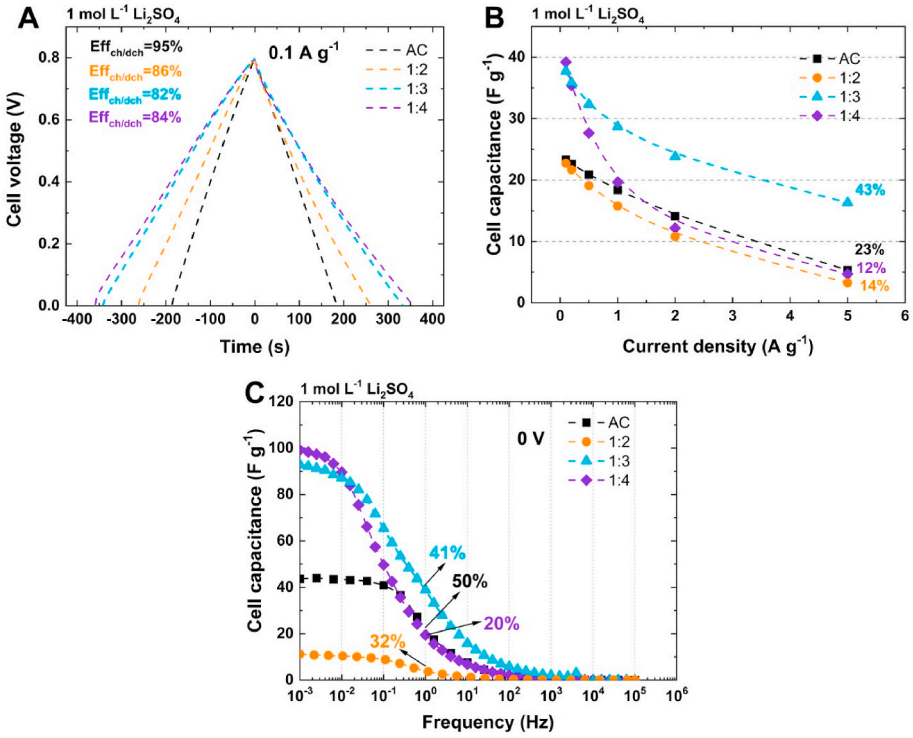

Fig. 4. Device characterization with 1 mol L^{-1} Li_2SO_4 and AC as positive electrode and negative electrode based on 1:2, 1:3 or 1:4 ACS: A) galvanostatic charge/discharge at 0.1 A g^{-1}; B) specific capacitance *vs.* current density; C) specific capacitance *vs.* frequency.

volume (0.14 cm^3 g^{-1}) and the widest micropore diameter (0.83 nm), but 12% rate handling suggests that ions more likely move towards easily available mesoporosity from micropore volume, loosing number of charged species at the electrode/electrolyte interface. The fibrous entangled morphology and the narrow optimal pore size distribution (0.83 nm) of AC [52] allow efficient and reversible ion adsorption. In the case of powdered carbon materials, the mesopore fraction is crucial for improving capacitance retention at high current loads [45,53].

Fig. 4C presents the evolution of the specific capacitance versus the frequency applied at 0 V in EIS studies. The data shown are in accordance with other electrochemical techniques. One can observe some specific behaviour of the 1:4 sample, probably related to the high burn-off of the material causing disorganization of the structure, as suggested by its lower content of Csp^2 (XPS data, Table S1, Supporting Information). The highest initial specific capacitance drops drastically, and at 1 Hz charge/discharge, only 20% of the capacitance is retained. The most stable among all studied ACS samples is 1:3, which in the EIS test demonstrates 42% specific capacitance retention at 1 Hz charge/discharge. AC is characterized by 50% capacitance retention in EIS studies. Taking into account the carbon composition (XPS spectra summarized in Table S1), a higher content of Csp^2 in the material (1:3–86.3%, 1: 4–82.5%) together with a higher nitrogen content (no nitrogen traces found for the 1:4 sample) guarantees satisfactory performance of 1:3 ACS in electrochemical impedance studies.

In accordance with other reported data, the specific capacitance found for ACS samples follows the trend: the more KOH used for the activation, the higher the capacitance at low regimes. However, considering the specific capacitance values at high current regimes, i.e., 5 A g^{-1}, the trend among the samples is no longer preserved.

In summary, a ratio of 1:3 appears to be the best compromise between structural, textural, and electrochemical characteristics with a suitable chemical composition (similar specific capacitance to 1:4) and very good rate performance comparable to AC system and higher than in the case of 1:4. Furthermore, the 1:3 sample is characterized by a lower burn-off of the material during the activation step, which ensures satisfactory textural properties after the activation process - the C-yield for each synthesis step has been presented in Table S2 (SI). The 1:3 ACS sample exhibits an optimal pore size and a balance between the volume of micro- (0.85 cm^3 g^{-1}) and mesopores (0.05 cm^3 g^{-1}) with a fair contribution of supermicropores (0.25 cm^3 g^{-1}). Therefore, a 1:3 CS: KOH ratio was selected as an optimal for further material optimization through the pyrolysis temperature.

3.2. *Impact of pyrolysis temperature on carbon properties and electrochemical performance*

Three pyrolysis temperatures were tested: 400 °C, 550 °C and 700 °C, and their influence on the morphology, texture or chemical composition of the ACS was investigated. Interestingly, as shown in Fig. 5, the temperature of the pyrolysis has a direct influence on the morphology of the sample after activation, and at high temperatures (higher than 550 °C), the spherical shape of the particles is preserved (Fig. 5A and B). The sample pyrolyzed at 400 °C lost the spherical morphology and shows a macroporous character (Fig. 5C), in which no traces of spherical particles remain.

The sample pyrolyzed at 550 °C shows a morphology that might be considered between samples T-700 and T-400, with a fraction of spherical particles but also a disordered macroporous material (Fig. 5B). The sample without activation and pyrolyzed at 600 °C was shown to maintain the spherical shape of the particles [16]. However, during activation, the materials pyrolyzed at lower temperatures (400 °C) are unstable and lose their morphology, explained by the fact that the organic polymer network does not fully convert to carbon at such a low temperature. The material is very rich in O- and N-functional groups [16] that are susceptible to inducing more interactions between the polymer and KOH than in the case of other samples. In addition, thermal decomposition at lower temperatures (400 °C) is accompanied by the release of several gases (CO, H_2O and H_2), as shown by mass spectrometry [16], which could contribute - in the presence of KOH - to loss of spherical morphology and its expansion to a random-like morphology

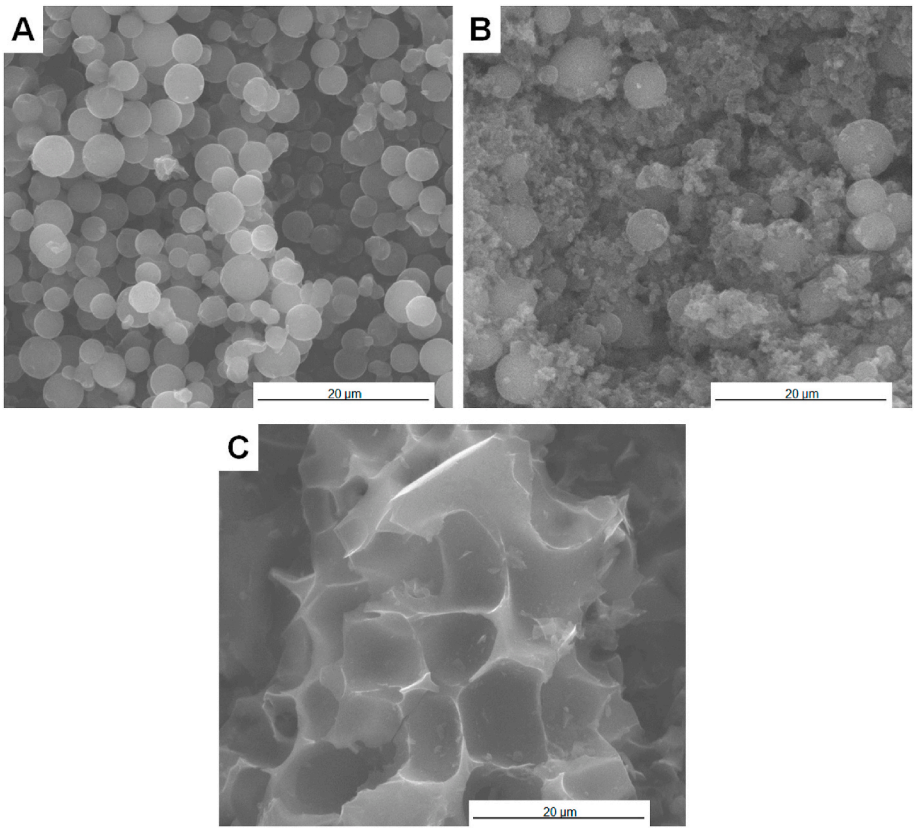

Fig. 5. SEM micrographs for carbon spheres pyrolyzed at different temperatures: A) 700 °C; B) 550 °C; C) 400 °C and activated at 750 °C with a 1:3 CS:KOH ratio.

with large macropores.

The textural and chemical surface properties of the obtained materials (presented in Table 2 and Table S3) are key parameters for evaluating the influence of the pyrolysis temperature on the characteristics of the ACS.

During synthesis, sulfur was added in the form of thiophene-2-carboxaldehyde, while nitrogen was sourced from TEDA (Fig. 1). Thus, the pyrolysis temperature decrease aimed at preservation of heteroatom doping (sulfur, nitrogen) in the surface chemistry of the ACS to boost their electrochemical performance with pseudocapacitive reactions. Surface chemistry was investigated using two methodologies: XPS – Table 2 and Fig. S2 (C1s deconvolution spectra of T-400 (Fig. S2A), T-550 (Fig. S2B) and T-700 (Fig. S2C) materials and N1s deconvolution spectra of T-400 (Fig. S2D) and EDX – Table S3. The results from both techniques seem to be in good agreement. Generally, the lower the pyrolysis temperature is, the higher the oxygen and the lower the carbon content in the samples. Carbonyl (C═O), ether (C-OR), and carboxylic (COOR) oxygen functional groups decorated the carbon surface (Fig. S2 A-C). However, N and S are rather randomly distributed among the samples.

Considering the XPS data, a decrease in the pyrolysis temperature preserves some sulfur content in the surface functionalities observed for the T-550 and T-400 samples. The S-heteroatom doping quantities, i.e., 0.3 at % (T-550) and 0.2 at % (T-400), are much lower than expected [32,54,55] but comparable to values reported in the literature (maximally 0.7 wt % of S) [29]. We believe that most of the S is lost during the activation step, which is carried out at higher temperatures (750 °C), since only the pyrolysis step allowed us to preserve much higher amounts in our previous work [32]. T-400 exhibits the highest N content (2.9 at %) when compared to T-700 (1.6 at %). Pyridinic (N═C-), pyridone (N═C–OH), quaternary (N^+-C) and nitrogen oxide (N^+-O) nitrogen functional groups are found on the surface of the T-400 sample (Fig. S2D). Thus, lowering the pyrolysis temperature positively impacts heteroatom doping.

The textural properties (Table 2 and Fig. 3) of the T-550 sample exhibit characteristics between samples T-400 and T-700, combining the properties of both. The pyrolysis temperature does not appear to directly influence the textural properties but rather the behaviour of the material during the activation step. Consequently, samples T-400, T-550 and T-700 demonstrate similar specific surface areas, i.e., 2115 $m^2\ g^{-1}$, 2430 $m^2\ g^{-1}$ and 2070 $m^2\ g^{-1}$, respectively. The pore volume is the most developed for the T-400 sample, owing to its macroporous open structure ($V_{TOTAL} = 1.09\ cm^3\ g^{-1}$). However, its micropore volume is not that much developed, showing the highest mesopore fraction among all materials (0.31 $cm^3\ g^{-1}$ – that stands as ca. 30% of a pore share in the total pore volume). For this sample, macropores (>100 nm) were also

Table 2
Properties (textural, surface chemistry measured by XPS) of carbons pyrolyzed at various temperatures (400 °C, 550 °C and 700 °C) and subsequently activated at 750 °C using a 1:3 carbon:KOH mass ratio.

Sample	N_2 adsorption at 77 K					CO_2 adsorption at 273 K	Chemical surface composition			
	S_{BET} $m^2\ g^{-1}$	S_{DFT} $m^2\ g^{-1}$	V_{TOTAL} $cm^3\ g^{-1}$	V_{MICRO} $cm^3\ g^{-1}$	V_{MESO} $cm^3\ g^{-1}$	V_{MICRO} $cm^3\ g^{-1}$	C at.%	O at.%	N at.%	S at.%
T-700	2070	1930	0.90	0.85	0.05	0.60	92.2	5.3	1.6	0.0
T-550	2430	1945	0.93	0.91	0.02	0.75	92.8	6.5	0.4	0.3
T-400	2115	1744	1.09	0.78	0.31	0.67	86.9	7.9	2.9	0.2

observed by SEM images. The total pore volume varies between the samples. T-550 and T-700 have similar total pore volumes, which are lower than the total pore volume of the T-400 sample. Thus, the pyrolysis temperature does not influence the micropore volume of the samples to a high extent – which can also be said about the specific surface area. However, a lower pyrolysis temperature induces a higher mesopore fraction and affects the morphology and surface chemistry.

The initial material screening was performed with 1 mol L^{-1} H_2SO_4 due to possible doping with S and its presumed activity in acidic media. To evaluate whether synthesized ACS demonstrated pseudocapacitance, electrode materials were first scanned in a three-electrode setup according to the experimental description (CV at 5 mV s^{-1} and wide potential screening was conducted using GITT with a current density ±50 mA g^{-1}). Figs. S4A–C shows the curves recorded for the T-400 electrode material. All synthesized carbons display similar electrochemical performance in three-electrode studies. Clearly, ACS is more stable in the negative potential range in aqueous acidic electrolytes. When potential range is limited to −0.2 V *vs*. NHE and 0.8 V *vs*. NHE, a rectangular cyclic voltammogram is recorded, indicating typical electrostatic attraction as a main charge storage mechanism (Fig. S4A). Exceeding the −0.2 V *vs. the* NHE potential value, a reduction peak appears (ca. −0.25 V *vs*. NHE) and corresponds to an oxidation peak ca. 0.4 V *vs*. NHE. According to the Pourbaix diagram for sulfur, the reduction peak can result from the presence of H_2S, S or HSO_4^- in the system. At acidic pH, sulfate anions are rich in possible redox reactions. Nevertheless, in the positive potential range – from E_{oc} towards higher potential values (Fig. S4B) – the carbon electrode operates more resistively and neither a redox contribution nor good charge propagation is observed. Thus, considering both potential ranges that resemble negative and positive electrode operational conditions, we recommend the use of synthesized ACS electrodes as negative electrodes in EC. The same conclusion can be drawn from Fig. S4C, where the electrode reaches the equilibrium state at a negative potential (−0.2 V *vs*. NHE). Furthermore, a safe operational voltage window for synthesized carbon in 1 mol L^{-1} H_2SO_4 was found to be equal to 1.2 V, which in the full device can be limited to ca. 1 V.

Fig. 6 presents electrochemical data for asymmetric ECs with synthesized carbons as negative electrode, AC as positive electrode operating with 1 mol L^{-1} H_2SO_4 and 1 mol L^{-1} Li_2SO_4 solutions. The AC:AC symmetric cell is shown as the reference electrochemical system. In all the systems tested with 1 mol L^{-1} H_2SO_4, the improvement in electrochemical performance was noticeable when ACS was used. Enhanced charge propagation is observed together with higher specific capacitance in a rectangular cyclic voltammetry shape (Fig. 6A). Sample T-550 presents the highest specific capacitance (56 F g^{-1} at 1 mV s^{-1}) with

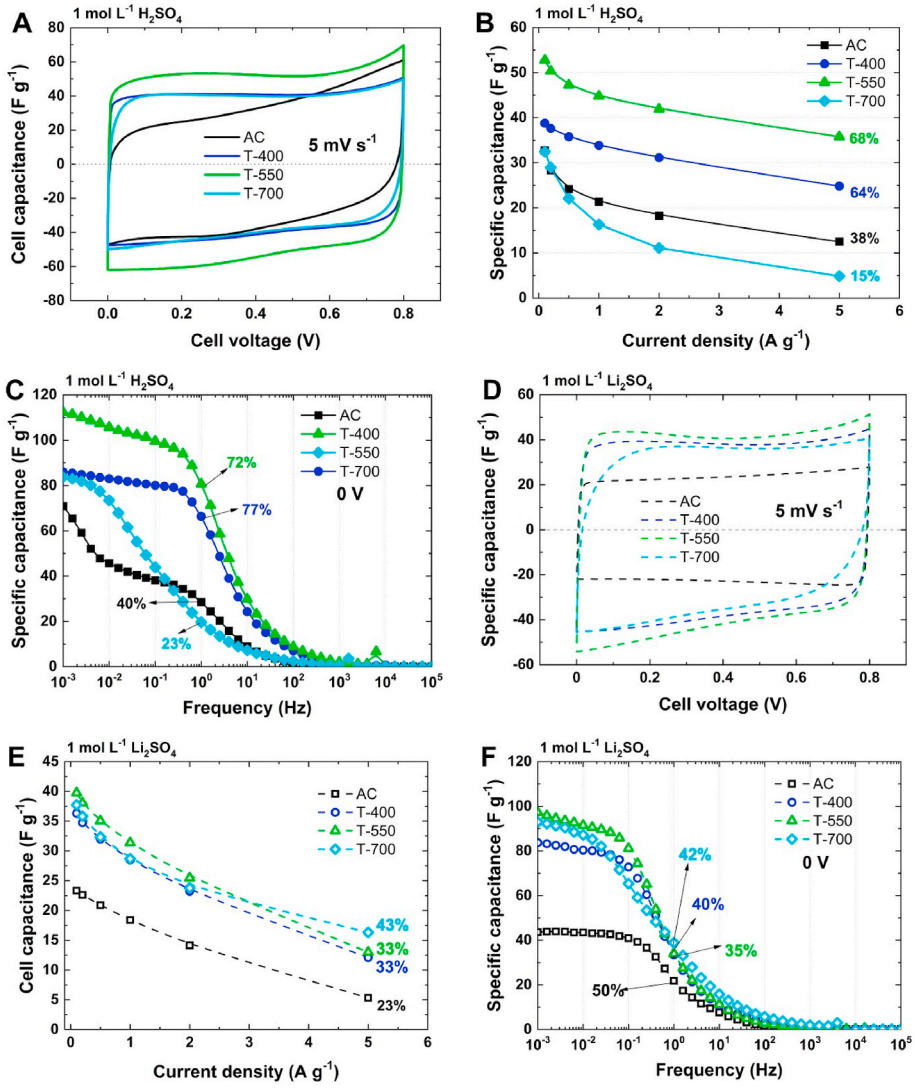

Fig. 6. Characterization of T-400, T-550, T-700 (−) electrodes and AC (+) electrodes in asymmetric cells and AC:AC symmetric cells in: 1 mol L^{-1} H_2SO_4: A) CV at 5 mV s^{-1}; B) rate capability from constant current charge/discharge; C) specific capacitance *vs*. frequency at 0 V; in 1 mol L^{-1} Li_2SO_4: D) cyclic voltammetry at 5 mV s-1; E) rate capability from constant current charge/discharge; F) capacitance *vs*. frequency at 0 V.

satisfactory rate handling (76%) (Fig. S5A). Samples T-400 and T-700 show specific capacitance values similar to each other at low scan rates (44 F g^{-1} at 1 mV s^{-1}); however, they are characterized by different rate handling capabilities. T-400 exhibited rate handling at 74%, while T-700 only 57%. All of these characteristics surpass those for the AC system, i.e., 47 F g^{-1} at 1 mV s^{-1} with 45% rate handling. The AC system exhibits moderate energetic efficiency of the charge/discharge process (69% at 0.1 A g^{-1}), visible in the charging curve shape (Fig. S4B). ACS-based systems are characterized by reversible charge/discharge processes with energetic efficiencies >84%. Their galvanostatic charge/discharge curves are triangular with Coulombic efficiencies higher than 90%. When a constant current charge/discharge is applied, sample T-700 is characterized by a lower rate handling (15%) than the AC reference system (38%). However, samples T-550 and T-400 show very good rate capability, at 64% (T-400) and 68% (T-550), respectively. The morphology and texture (Fig. 5) of spherical, dense particles do not appear to facilitate rate handling, as the macroporous T-400 material and the mixed T-550 (macroporous and spheres) demonstrate better performance.

All electrochemical data (potentiodynamic and potentiostatic) are in agreement, as is electrochemical impedance spectroscopy at 0 V, likewise (Figs. 6C and S5C). Rate handling (specific capacitance calculated at 1 Hz to that at 1 mHz) follows the trend from the highest value to the lowest value: T-400 (77%) ~ T-550 (72%) > AC (40%) > T-700 (23%). Samples T-400 and T-550 are again noted to demonstrate very similar electrochemical performance even though their morphology differs. Thus, the combination of morphology, texture properties, and surface chemistry is responsible for the electrochemical performance of ACS electrodes. ACS samples are characterized by a plateau of specific capacitance in the low frequency range (Fig. 6C), indicating charge accumulation in the electric double layer. Interestingly, the time constant of the synthesized carbon systems follows the trend: 1.27 s (T-550) < 1.59 s (T-700) and 2.41 s (T-400). The time constant appears to depend on the morphology and carbon content in the samples, as T-550 and T-700 display similar response times. T-400, which is composed of a macroporous texture, has the longest response time. The trend of response time perfectly matches the carbon content among the samples (Table 2). T-550 shows 92.2 at. %, T-700 shows 92.8 at.% and their response times are comparable. Sample T-400, with a content of 86.9 at. % carbon, together with rich surface chemistry (containing nitrogen and sulfur), displays the longest response time.

A typical capacitive character is reflected in the Nyquist plot (Fig. S5C). The AC-based system shows the worst electrochemical performance in this study. ECs with T-400 and T-550 do not demonstrate a well-developed Warburg region; therefore, the electric double layer is not limited by diffusion [56]. The ESR (equivalent series resistance at 100 kHz) recorded for EC is similar for T-400 (0.35 Ω), T-550 (0.28 Ω) and AC (0.40 Ω). The T-700 cell shows slightly higher resistance equal to 0.59 Ω. However, all cells are characterized by moderate resistance values compared to the resistance values in the literature [26].

To verify whether the synthesized carbon material can be used in neutral ECs, it was combined with a 1 mol L^{-1} Li_2SO_4 electrolytic solution (Fig. 6D–F). The symmetric AC:AC system demonstrates purely capacitive behaviour, visible in the rectangular cyclic voltammetry profile (Fig. 6D), triangular charge/discharge curve (Fig. S6) and plateau of specific capacitance in the low frequency region in the EIS measurement (Fig. 6F). Qualitatively, synthesized carbons (T-400 and T-550) are comparable to AC-based systems in neutral media (what can be observed in, e.g., rectangular cyclic voltammograms or similar specific capacitance trend *vs.* frequency). However, they exceed the performance of symmetric AC:AC cells with capacitance values (Fig. 6E). Their specific capacitance and rate handling are worse when 1 mol L^{-1} Li_2SO_4 is applied as an electrolyte instead of 1 mol L^{-1} H_2SO_4, as it is assumed that the lower conductivity of the aqueous solution of Li_2SO_4 is at the origin of this result [57].

A convenient comparison of the electrochemical performance of the materials in two electrolytes, investigated at the full cell level is presented in the Ragone plot (Fig. S7). Briefly, in acidic environment (1 mol L^{-1} H_2SO_4, Fig. S7a), EC with electrodes made from T-400 and T-550, demonstrate an improved power response. Their energy is also improved compared to the commercial AC, however, the most notable difference between materials can be observed at high power loads. In case of neutral electrolyte (1 mol L^{-1} Li_2SO_4, Fig. S7b) the power response is not remarkably improved, as the limiting factor is the conductivity of aqueous electrolytic solutions. Nevertheless, in comparison to AC, synthesized materials doubled the amount of energy stored.

However, this cannot be the only reason considering that in H_2SO_4, the electrochemical performance is strongly material dependent, while in Li_2SO_4, fewer performance differences are observed *vs.* the electrode material. To obtain more insights into this behaviour, wettability measurements were performed in contact with applied electrolytic solutions. Moreover, electronic conductivity measurements were conducted on the composite electrodes as depicted below.

Smaller contact angles (Fig. 7) are observed when electrode materials are combined with acidic electrolyte, e.g., for T-400, the contact angles are 64° (1 mol L^{-1} H_2SO_4) and 120° (1 mol L^{-1} Li_2SO_4). As in both electrolytes the anion is the same (SO_4^{2-}), the difference in wettability may be associated with the size of the cation (Li^+ has a larger diameter than H^+) or viscoelastic properties of the solution. Moreover, increasing the pyrolysis temperature increases the contact angle measured for both electrolytic solutions. This increase is more significant in H_2SO_4 (64–126° for T-400 and N-A materials, respectively) than for Li_2SO_4 (120–136° for T-400 and N-A materials, respectively) because the rate handling of the T-400 material is always better than the rate handling of T-700. Therefore, the combination of morphology, texture (meso- and macroporosity) and surface content (especially oxygen content) is herein a crucial factor. Samples T-700 and N-A have different textural properties and conductivities, but the same morphologies are characterized by similar high contact angles. Macroporous structures absorb aqueous solutions better than spherical and compact particles; thus, electrodes are better soaked. Sample T-550 demonstrates physicochemical features between the T-400 and T-700 materials, with a synergistic effect between the sample morphology, surface functionalities, and textural properties – resulting in the best electrochemical performance. In terms of rate handling, the samples T-400 and T-550 seem to be very comparable. In summary, the requirements in terms of material properties to achieve good performance are different depending on the electrolyte selected. For H_2SO_4, meso-macroporosity is important to ensure good wettability with the electrolyte, while for Li_2SO_4, the morphology does not appear to be an important factor.

The conductivity of the electrode material appears to be not directly related to morphology, as samples N-A and T-700 exhibiting the same spherical morphology differ significantly (3 mS cm^{-1} *vs.* 212 mS cm^{-1}). Thus, the conductivity can be more related to the structure and chemical composition. Interestingly, the high electric conductivity value of the T-700 sample does not guarantee the high power capability of this material in the full device.

Therefore, physicochemical tests (Fig. 7) prove the statement that an optimal combination of surface functionality, morphology, and texture is crucial for ECs applications. Moreover, all the above-mentioned parameters affect electrochemical performance differently in acidic and neutral media. Acidic surface functionalities (Tables 2 and S3) ensure a good matching with acidic, highly conductive electrolytes, especially when sulfur heteroatom doping occurs. As a consequence, the same materials matched together with a neutral lithium sulfate solution resulted in slightly worse electrochemical performance. Moreover, one cannot neglect the electrolytic solution features itself, as 1 mol L^{-1} H_2SO_4 is much more conductive than 1 mol L^{-1} Li_2SO_4.

The volumetric characteristics of the synthesized carbons were also considered. The composite electrode density of the T-400, T-550, and T-700 materials was calculated (based on the thickness, geometrical diameter, and mass of prepared electrode discs in the probe of 10

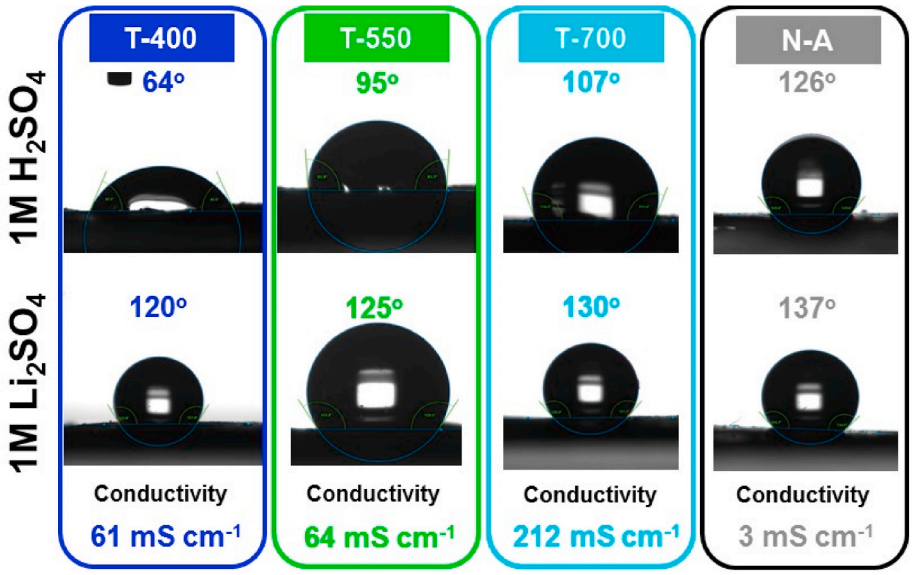

Fig. 7. Contact angle measurements of electrode materials: T-400, T-550, T-700 and N-A with 1 mol L^{-1} H_2SO_4 (upper line) and 1 mol L^{-1} Li_2SO_4 (bottom line). The electronic conductivity of the electrode composite measured at 100 kHz is presented as the inset.

samples). Therefore, the T-400 electrode material exhibits densities equal to 0.66 g cm^{-3}, T-550– 0.48 g cm^{-3} and T-700–0.68 g cm^{-3}. Moreover, such electrode density values can be explained by various packing abilities related to the structure (graphitic domains) with textural properties of the material and different chemical compositions of each ACS material. The values are in the range discussed in the literature [29]. The reference AC used for comparison purposes is 0.64 g cm^{-3}. To recalculate the specific capacitance of the asymmetric devices, the average density of both electrodes was considered. Thus, the volumetric and gravimetric characteristics of asymmetric devices are improved compared to the characteristics of AC:AC systems. Interestingly, the T-550-based system shows 53 F g^{-1}, which equals 30 F cm^{-3} in 1 mol L^{-1} H_2SO_4 at 0.1 A g^{-1}. The specific capacitance recorded for the T-550-based system is 60% higher than the specific capacitance of the AC:AC system (33 F g^{-1}) and +43% considering its volumetric capacitance (21 F cm^{-3} for the AC:AC system). In 1 mol L^{-1} Li_2SO_4, the situation is analogous – application of an ACS negative electrode improves the specific and gravimetric metrics of the full device compared to the symmetric AC:AC electrode. T-550-based EC exhibits 40 F g^{-1} = 22 F cm^{-3}, which represents a +74% and +47% increase compared to the

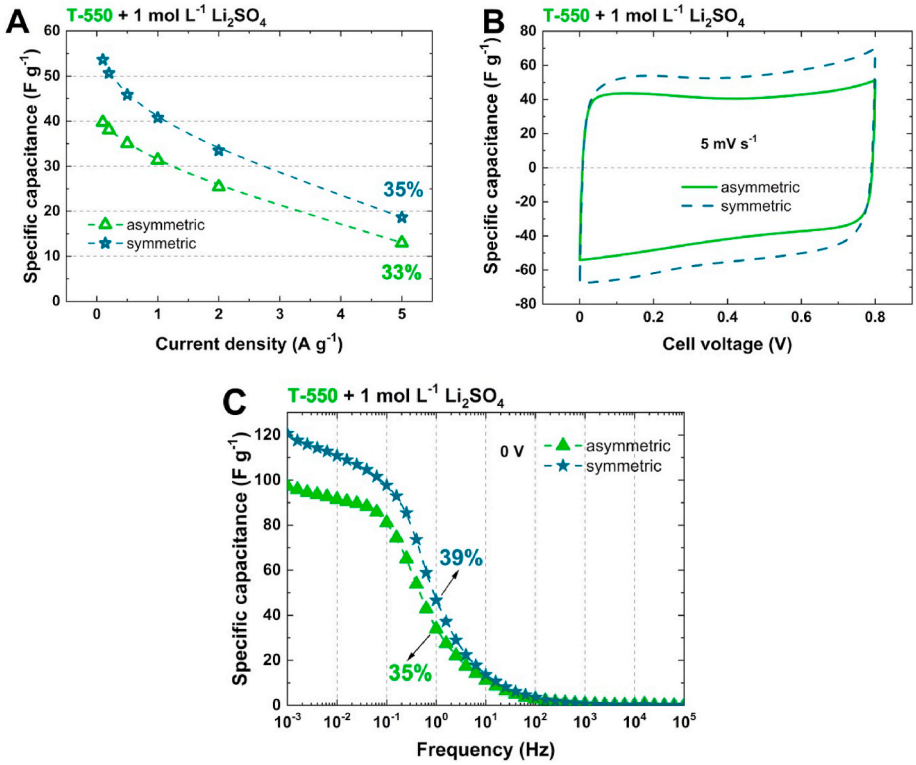

Fig. 8. T-550 electrode material tested in asymmetric and symmetric cells with 1 mol L^{-1} Li_2SO_4: A) specific capacitance *vs.* current density; B) cyclic voltammetry at 5 mV s^{-1}; C) specific capacitance *vs.* frequency.

AC:AC system (23 F g^{-1} = 15 F cm^{-3}).

Specific capacitance can also be discussed considering the S_{BET} of electrode materials, giving values in μF cm^{-2}. In acidic medium, the materials reveal at 0.1 A g^{-1}: 72 μF cm^{-2} (T-400), 88 μF cm^{-2} (T-550), 60 μF cm^{-2} (T-700) and 72 μF cm^{-2} (AC:AC). Only T-550 surpasses the specific capacitance value (in μF cm^{-2}) obtained by the AC:AC system. In a neutral electrolytic solution, all synthesized carbons exceeded the performance of the AC: AC device (52 μF cm^{-2}), with 68 μF cm^{-2} (T-400), 64 μF cm^{-2} (T-550), and 72 μF cm^{-2} (T-700). The gravimetric and volumetric specific capacitance values are on the level reported for various carbon materials in aqueous electrolytic solutions [26], proving that challenging synthesis of micro-mesoporous spherical carbons for EC application was successfully conducted. The optimal combination of the morphology, texture, and surface chemistry of ACS plays an important role in the optimization of AC:AC device performance in aqueous electrolytes and was successfully obtained for T-550 samples.

Additionally, sample T-550 was also implemented in the symmetric EC device to verify whether synthesized materials can play the role of a negative electrode only or are a suitable material for symmetric cell construction. Fig. 8 presents data for asymmetric and symmetric ECs based on the T-550 electrode material.

The symmetric configuration was verified in both acidic and neutral media; however, for the sake of comparison, Fig. 8 shows only data with 1 mol L^{-1} Li_2SO_4 as this electrolyte is more promising in EC applications. The specific capacitance recorded in the low current regime or slow scan rates is even higher than the specific capacitance recorded for the asymmetric system (Fig. 8A. Nevertheless, the rate handling for both systems is maintained on the same level, i.e., 50% from cyclic voltammetry (Fig. 8B), 35% from galvanostatic studies, and 39% from impedance spectroscopy (Fig. 8C). Thus, both systems operate at satisfactory levels, and synthesized T-550 carbon can be used as an active material in both electrode compositions, which can beneficially influence the possible manufacturing process (assembly time and cost).

On the basis of the specific capacitance values and the power response, ACS seems to be promising for the EC application in both acidic and neutral media. Their qualitative performance is very satisfactory, with a specific capacitance exceeding the specific capacitance of a system based on commercial AC. In summary, synthesized ACSs have great potential in energy storage devices, and, because of improvements in their initial features (compared to those of N-A material), they reveal parameters suitable for ECs.

4. Conclusions

The synthesis of porous carbon materials for electrochemical capacitor application was successfully realized. Two synthesis parameters were elucidated: pyrolysis temperature (400 °C, 550 °C and 700 °C) and carbon:KOH ratio (from 1:2 to 1:4) in the activation process. The spherical morphology of the carbon materials was obtained after pyrolysis at 700 °C and activation at 750 °C independently of the carbon: KOH ratio. This ratio mainly influences the textural properties of ACS materials. The specific surface area, together with micropore volume and average pore size, is increasing for samples using higher carbon: KOH ratios (from N-A to 1:4), which induce a capacitance at low regimes. However, at high current regimes, the trend among the samples is no longer preserved. The carbon obtained with a 1:3 carbon:KOH ratio reveals the best electrochemical performance with a compromise of the amount of KOH used. The structural characteristics of this material, i.e., higher Csp^2 and N content can explain the better results compared to 1:4 carbon:KOH.

The temperature of pyrolysis affects the final morphology of the sample, and the spherical morphology (700 °C) gradually shifts to a random morphology with macroporous texture at lower temperatures (400 °C, 550 °C). The presence of small mesopores or even macropores in low-temperature pyrolyzed samples improves charge propagation, especially in acidic 1 mol L^{-1} H_2SO_4. The structure and chemical composition of ACS impacts their conductivity and, consequently, their response time. The macropore texture and rich surface chemistry (T-700) lead to an increase in response time. Conductivity studies themselves prove that materials exhibiting good conductivity do not necessarily ensure good charge propagation; the electrode morphology/texture and electrode/electrolyte interface are the key factors.

Both surface chemistry and morphology impact the ACS electrode wettability (particularly in acidic medium). T-400 possessing rich functionalities and meso/macropores exhibits the best wetting properties.

In summary, ACS can be successfully applied in both acidic and neutral aqueous media with electrochemical performance superior to that of symmetric AC:AC reference devices. Moreover, ACS can be used in asymmetric and symmetric cell construction. The synergetic effect was obtained for the T-550 material. Its textural properties that combine a large surface area and optimal pore size, surface chemistry, and morphology (preserved spheres mixed with open macrostructure) lead to the best electrochemical performance among synthesized ACS. ECs based on T-550 exhibit 31 F g^{-1} per system with 1 mol L^{-1} Li_2SO_4, while the symmetric AC: AC cell exhibits only 18 F g^{-1} at 1 A g^{-1}. Furthermore, ACS shows good charge propagation and capacitance retention (>60%) in an acidic medium (1 mol L^{-1} H_2SO_4) compared to the reference AC:AC symmetric cell (38%).

CRediT authorship contribution statement

Anetta Platek-Mielczarek: validation, Formal analysis, Investigation, Resources, Writing – original draft, Visualization, Funding acquisition. **Joanna Conder:** Conceptualization, Validation, Formal analysis, Resources. **Krzysztof Fic:** Conceptualization, Methodology, Resources, Writing – review & editing, Supervision, Project administration, Funding acquisition. **Camelia Matei Ghimbeu:** Conceptualization, Methodology, Resources, Writing – review & editing, Supervision, Project administration, Funding acquisition.

Declaration of competing interest

The authors declare that they have no known competing financial interests or personal relationships that could have appeared to influence the work reported in this paper.

Acknowledgements

The authors acknowledge the European Commission and the European Research Council for financial support by the Starting Grant project (GA 759603) under the European Union's Horizon 2020 Research and Innovation Programme. APM obtained financial funding in the form of a doctoral scholarship from the National Science Centre (2019/32/T/ST4/00276) and the programme im. Iwanowskiej from the National Agency for Academic Exchange.

This work was performed in the framework of RS2E (French research network on electrochemical energy storage) and the laboratory of excellence for electrochemical energy storage, STORE-EX. Moreover, the authors acknowledge Philippe Fioux (XPS analysis), Adrian Beda (SEM, MEB/EDX), Cyril Vaulot (adsorption data) and Philippe Kunemann (contact angle measurements) for technical help within the IS2M platforms.

Appendix A. Supplementary data

Supplementary data to this article can be found online at https://doi.org/10.1016/j.jpowsour.2022.231714.

References

[1] J.Y. Zhao, A.F. Burke, Energy Storage Mater. 36 (2021) 31–55.

[2] G. Moussa, C.M. Ghimbeu, P.L. Taberna, P. Simon, C. Vix-Guterl, Carbon 105 (2016) 628–637.
[3] M.M. Hantel, D. Weingarth, R. Kotz, Carbon 69 (2014) 275–286.
[4] L.H. Wang, M. Fujita, M. Inagaki, Electrochim. Acta 51 (2006) 4096–4102.
[5] B. Kruner, J. Lee, N. Jackel, A. Tolosa, V. Presser, ACS Appl. Mater. Interfaces 8 (2016) 9104–9115.
[6] Y.Z. Jin, Y.J. Kim, C. Gao, Y.Q. Zhu, A. Huczko, M. Endo, H.W. Kroto, Carbon 44 (2006) 724–729.
[7] J. Ding, H. Zhang, H. Zhou, J. Feng, X. Zheng, C. Zhong, E. Paek, W. Hu, D. Mitlin, Adv. Mater. 31 (2019) 1970217–n/a.
[8] A.D. Roberts, X. Li, H. Zhang, Chem. Soc. Rev. 43 (2014) 4341–4356.
[9] Z.M. Shen, J. Du, Y.H. Mo, A.B. Chen, Carbon 173 (2021) 22–30.
[10] Z. Wang, Y. Li, J. Liu, T. Gui, H. Ogata, W. Gong, A.K. Vipin, Y. Wang, G.J. Hong Melvin, J. Ortiz-Medina, S. Wang, R. Cruz-Silva, S. Morimoto, Y. Hashimoto, B. Fugetsu, I. Sakata, M. Terrones, M. Endo, Carbon 167 (2020) 11–18.
[11] Q. Zhang, L. Li, Y.L. Wang, Y.J. Chen, F. He, S.L. Gai, P.P. Yang, Electrochim. Acta 176 (2015) 542–547.
[12] S.K. Kim, E. Jung, M.D. Goodman, K.S. Schweizer, N. Tatsuda, K. Yano, P.V. Braun, ACS Appl. Mater. Interfaces 7 (2015) 9128–9133.
[13] N.P. Wickramaratne, J.T. Xu, M. Wang, L. Zhu, L.M. Dai, M. Jaroniec, Chem. Mater. 26 (2014) 2820–2828.
[14] S. Chen, G. Yang, X. Zhao, N. Wang, T. Luo, X. Chen, T. Wu, S. Jiang, P.A. van Aken, S. Qu, T. Li, L. Du, J. Zhang, H. Wang, H. Wang, Front. Chem. 8 (2020) #663.
[15] Y. Yamada, T. Sasaki, N. Tatsuda, D. Weingarth, K. Yano, R. Kotz, Electrochim. Acta 81 (2012) 138–148.
[16] A. Maetz, L. Delmotte, G. Moussa, J. Dentzer, S. Knopf, C.M. Ghimbeu, Green Chem. 19 (2017) 2266–2274.
[17] N. Deka, J. Barman, J. Deka, K. Raidongia, G.K. Dutta, Chemelectrochem 6 (2019) 3327–3336.
[18] Y. Wang, Q.M. Dai, L.T. Yang, Y. Liu, C.Z. Yu, C. Yao, X. Xu, J. Electroanal. Chem. 873 (2020), 114462.
[19] W.J. Lu, M.X. Liu, L. Miao, D.Z. Zhu, X. Wang, H. Duan, Z.W. Wang, L.C. Li, Z.J. Xu, L.H. Gan, L.W. Chen, Electrochim. Acta 205 (2016) 132–141.
[20] J. Wang, C. Ma, L. Su, L. Gong, D. Dong, Z. Wu, Chemelectrochem 7 (2020) 4606–4613.
[21] H.R. Wang, H.W. Zhou, M. Gao, Y.A. Zhu, H.T. Liu, L. Gao, M.X. Wu, Electrochim. Acta 298 (2019) 552–560.
[22] S. Wu, Y. Xue, Q.L. Yang, Q.Z. Hu, T. Cui, Q. Su, F.P. Yin, Y.B. Wang, H.Y. Zhan, Diam. Relat. Mater. 111 (2021), 108187.
[23] Y. Liu, X.Y. Cai, B.F. Luo, M. Yan, J.H. Jiang, W.D. Shi, Carbon 107 (2016) 426–432.
[24] K.W. Shen, F. Ran, X.X. Zhang, C. Liu, N.J. Wang, X.Q. Niu, Y. Liu, D.J. Zhang, L. B. Kong, L. Kang, S.W. Chen, Synthetic Met 209 (2015) 369–376.
[25] Z.B. Lei, J.T. Zhang, X.S. Zhao, J. Mater. Chem. 22 (2012) 153–160.
[26] C. Moreno-Castilla, Adv. Colloid Interface Sci. 236 (2016) 113–141.
[27] S. Chen, G. Yang, X. Zhao, N. Wang, T. Luo, X. Chen, T. Wu, S. Jiang, P.A. van Aken, S. Qu, T. Li, L. Du, J. Zhang, H. Wang, H. Wang, Front. Chem. 8 (2020) 663.
[28] X.M. Ma, M.X. Liu, L.H. Gan, Y.H. Zhao, L.W. Chen, J. Solid State Electrochem. 17 (2013) 2293–2301.
[29] Y.-L. Dang, J.-P. Cao, Z.-Q. Hao, Y. Wu, X.-Y. Zhao, Q.-Q. Zhuang, Z. Zhou, X.-Y. Wei, Waste Biomass Valori 11 (2019) 4429–4440.
[30] J. Xu, S. Zhang, Z. Wei, W. Yan, X. Wei, K. Huang, J. Colloid Interface Sci. 585 (2021) 12–19.
[31] Y. Dong, H. Niu, H.M. Lin, F.Y. Qu, J. Nano Res. 22 (2020) #283.
[32] A. Martínez de Yuso, M. De Fina, C. Nita, P. Fioux, J. Parmentier, C. Matei Ghimbeu, Microporous Mesoporous Mater. 243 (2017) 135–146.
[33] S.B. Liu, Y. Zhao, B.H. Zhang, H. Xia, J.F. Zhou, W.K. Xie, H.J. Li, J. Power Sources 381 (2018) 116–126.
[34] W. Sun, Y.L. Zhang, F.Q. Yang, Electrochim. Acta 357 (2020), 136874.
[35] L. Mao, Y. Zhang, Y.T. Hu, K.H. Ho, Q.Q. Ke, H.J. Liu, Z.G. Hu, D. Zhao, J. Wang, RSC Adv. 5 (2015) 9307–9313.
[36] J.J. Yan, L. Miao, H. Duan, D.Z. Zhu, Y.K. Lv, W. Xiong, L.C. Li, L.H. Gan, M.X. Liu, Electrochim. Acta 358 (2020), 136899.
[37] L. Miao, D.Z. Zhu, Y.H. Zhao, M.X. Liu, H. Duan, W. Xiong, Q.J. Zhu, L.C. Li, Y. K. Lv, L.H. Gan, Microporous Mesoporous Mater. 253 (2017) 1–9.
[38] J.G. Wang, H.Z. Liu, H.H. Sun, W. Hua, H.W. Wang, X.R. Liu, B.Q. Wei, Carbon 127 (2018) 85–92.
[39] A. Beda, F. Rabuel, M. Morcrette, S. Knopf, P.L. Taberna, P. Simon, C.M. Ghimbeu, J. Mater. Chem. 9 (2021) 1743–1758.
[40] J. Jagiello, A. Chojnacka, S.E.M. Pourhosseini, Z. Wang, F. Beguin, Carbon 178 (2021) 113–124.
[41] B. Zdravkov, J. Čermák, M. Šefara, J. Janků, Open Chemistry 5 (2007) 385–395.
[42] M. Thommes, K. Kaneko, A.V. Neimark, J.P. Olivier, F. Rodriguez-Reinoso, J. Rouquerol, K.S.W. Sing, Pure Appl. Chem. 87 (2015) 1051–1069.
[43] C. Vix-Guterl, E. Frackowiak, K. Jurewicz, M. Friebe, J. Parmentier, F. Beguin, Carbon 43 (2005) 1293–1302.
[44] C.A. Schneider, W.S. Rasband, K.W. Eliceiri, Nat. Methods 9 (2012) 671–675.
[45] A. Platek-Mielczarek, C. Nita, C. Matei Ghimbeu, E. Frackowiak, K. Fic, ACS Appl. Mater. Interfaces 13 (2021) 2584–2599.
[46] K.C. Kim, T.U. Yoon, Y.S. Bae, Microporous Mesoporous Mater. 224 (2016) 294–301.
[47] V. Presser, J. McDonough, S.H. Yeon, Y. Gogotsi, Energy Environ. Sci. 4 (2011) 3059–3066.
[48] C. Largeot, C. Portet, J. Chmiola, P.L. Taberna, Y. Gogotsi, P. Simon, J. Am. Chem. Soc. 130 (2008) 2730–2731.
[49] A. Platek, C. Nita, C.M. Ghimbeu, E. Frackowiak, K. Fic, Electrochim. Acta 338 (2020), 135788.
[50] S. Kondrat, C.R. Perez, V. Presser, Y. Gogotsi, A.A. Kornyshev, Energy Environ. Sci. 5 (2012) 6474–6479.
[51] F. Béguin, E. Frąckowiak, Carbons for Electrochemical Energy Storage and Conversion Systems, CRC Press, New York, 2009.
[52] K. Fic, A. Platek, J. Piwek, E. Frackowiak, Mater. Today 21 (2018) 437–454.
[53] V.S. Bhat, S. S, T.J. Jayeoye, T. Rujiralai, U. Sirimahachai, K.F. Chong, G. Hegde, Nano Select 1 (2020) 226–243.
[54] R.Y. Luan, D. Xu, H. Pan, C.L. Zhu, D.W. Wang, X. Meng, Y. Li, M. Imtiaz, S.M. Zhu, J. Ma, J. Energy Storage 22 (2019) 60–67.
[55] W.G. Feng, E. Borguet, R.D. Vidic, Carbon 44 (2006) 2990–2997.
[56] B.-A. Mei, O. Munteshari, J. Lau, B. Dunn, L. Pilon, J. Phys. Chem. C 122 (2017) 194–206.
[57] K. Fic, A. Platek, J. Piwek, J. Menzel, A. Slesinski, P. Bujewska, P. Galek, E. Frackowiak, Energy Storage Mater. 22 (2019) 1–14.